Receiver Design of Radio-Controlled Clocks Based on the New WWVB Broadcast Format

Yingsi Liang, *Student Member, IEEE*, Oren Eliezer, *Senior Member, IEEE*, and Dinesh Rajan, *Senior Member, IEEE*

Abstract—The architecture and algorithms for the first all-digital radio-controlled clock receiver for the new WWVB broadcast format are proposed. To address the potentially low signal-to-noise ratio conditions and the relatively large frequency offsets experienced in the receiver, two alternative timing synchronization approaches are investigated, i.e., one based on a maximum-likelihood (ML) criterion and the other based on correlation. We show that the correlation-based synchronization technique reduces the implementation complexity by over 50%, while its performance is only less than 1 dB inferior to that of the ML-based technique. Decision and detection algorithms are proposed for two operating regimes in the receiver: tracking and acquisition. In tracking, the proposed decision strategies reduce the timing mean squared error by as much as 63% compared with what the synchronizer produces without any additional processing. In acquisition, the proposed joint synchronization and decoding technique significantly improves the robustness by exploiting the channel code in the data. Compared with receivers based on the legacy broadcast, over 15 dB performance gains are achieved by the modulation and algorithms proposed for the tracking and acquisition operations. In addition to reception performance analyses, energy consumption tradeoffs are also presented.

Index Terms—WWVB, time signal broadcast, ratio-controlled clock, receiver design, synchronization, tracking, acquisition.

I. INTRODUCTION

WWVB is the US government's time code radio station located near Fort Collins, Colorado. It is operated by the National Institute of Standards and Technology (NIST) based on a high-precision atomic clock. The station continuously broadcasts digitally represented time information, including year, day, hour, minute, and leap second and daylight saving time (DST) notices. Millions of radio-controlled clocks (RCCs) throughout North America are synchronized to the station and benefit from accurate time keeping and automatic adjustments for DST. Currently, two co-existing broadcast formats are used by WWVB. The legacy broadcast format, introduced in 1965, using amplitude modulation (AM) and pulse-width modulation (PWM), was designed to enable the use of a low-cost envelope detection based receiver with minimal processing to decipher the message at the cost of poor performance [1].

The new broadcast format, based on the addition of phase modulation (PM) to the carrier, was introduced in 2012. While maintaining backward compatibility, the new modulation scheme offers a performance gain of approximately 10 dB if optimal receivers are considered in both broadcast formats. However, while the proposed receiver for the PM signal is demonstrated to have near-optimal performance, the receivers for the legacy broadcast are typically based on envelope detectors, resulting in an even larger performance gap of at least 12 dB between the legacy and new broadcast formats [1]. Further, there are different transmission modes in the new broadcast format, having different bit rates and frame durations, and thus supporting different signal-to-noise ratio (SNR) ranges, further increasing the performance gap to several orders of magnitude [2], [3]. Among all transmission modes, the *Normal mode* is transmitted most frequently, and most receivers within the continental US experience sufficient SNR to recover the data successfully in this mode, particularly during nighttime or in the absence of excessive shielding losses and interference. Therefore, this paper focuses on the reception of Normal mode in the PM broadcast.

For both the legacy format and the new format in Normal mode, the bit rate is 1 bit/sec and the frame duration is one minute. The baseband pulse shapes for the "0", "1" and marker symbols in the legacy format are shown in Fig. 1. The marker symbol is used for timing only, and does not carry any information. The information bits "0" and "1" differ only in their pulse widths. In contrast, in the new binary-phase-shift-keying (BPSK) based broadcast format, bit "0" and bit "1" are distinguished by phase and are antipodal. Bit "0" maintains the carrier phase, corresponding to the same waveforms shown in Fig. 1, whereas bit "1" will reverse the carrier phase by 180°, corresponding to negating the waveforms shown in Fig. 1 [2], [3].

In addition to its improved modulation scheme, the new PM format also introduces a synchronization word that supports a tracking operation at the receiver, allowing reduced receiver power consumption. The acquisition operation is performed when the RCC is first powered or reset, at which time it needs to recover the information bits and decode the time information. After successful acquisition, RCC devices may perform tracking periodically to compensate for the timing drift caused by the frequency inaccuracy of their crystal.

Due to the nature of the time broadcast and its applications, there are various receiver design challenges and considerations that are unique to the WWVB RCC receivers. First, the receiver should be able to operate at very low SNR conditions, since high levels of man-made noise (MMN) and shielding losses are likely in many scenarios. Second, the relative frequency
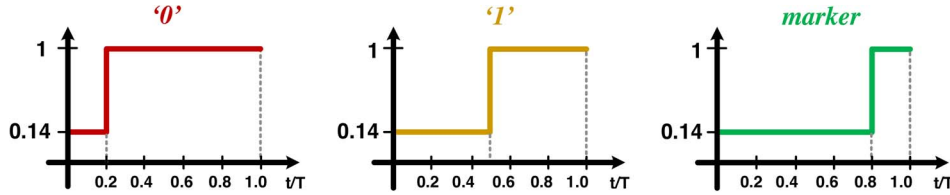
Fig. 1.   Baseband signal waveforms of the legacy AM/PWM WWVB broadcast.
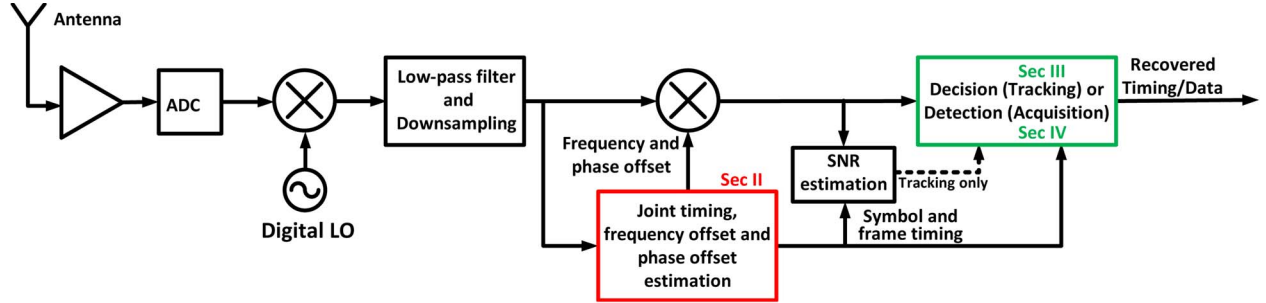

Fig. 2.   Block diagram of the proposed digital receiver for the new BPSK-based broadcast format.

offset at the receiver is large due to the long symbol duration, complicating coherent detection. Third, the receiver should have low implementation complexity to be suitable for low-cost consumer market devices. Lastly, receiver energy consumption should also be minimized for battery operated devices.

The main contributions of this paper are as follows:

- We present the architecture and performance of the first all-digital RCC receiver based on the new WWVB broadcast format. Compared with the conventional envelope detection based RCC devices for the legacy broadcast format, the proposed receiver demonstrates over 15 dB performance gain.
- We propose a maximum likelihood (ML) based timing synchronization algorithm in the presence of very large frequency errors ($\Delta f \leq 4\frac{1}{T}$). Further, various approximations are made to reduce the computational complexity of the synchronization algorithm. Specifically, we show that the correlation based approach reduces the implementation complexity by over 50%, at the cost of less than 1 dB of performance degradation when compared with the optimal algorithm.
- Two receiver operating regimes are studied; i) In tracking, both optimal Minimum Mean Square Error (MMSE) and reduced-complexity decision strategies are studied. If only a single reception attempt is made, simulation results show that either decision algorithm can reduce the timing MSE by as much as 63% compared with the MSE at the output of the synchronizer, while the reduced complexity algorithm performs very close to the MMSE algorithm. We also show how the MSE can be further reduced by allowing multiple receptions at sufficiently high SNR. Despite the inaccuracy of SNR estimation under low SNR conditions, the MMSE algorithm that allows multiple receptions can maintain a low timing MSE. ii) In acquisition, the joint synchronization and decoding improves the robustness by exploiting the channel code in the data. Simulation results show that a sufficiently low probability of false detection, on the order of 10^{-4}, can be reached at 8 dB SNR, for

which the time information can be successfully decoded at a probability as high as 98%.
- Receiver design tradeoffs between energy consumption and performance are presented for both the tracking and acquisition operations. During tracking, setting time search interval t_s to the maximum timing drift can include all possible timing drift in the time search operation, at the cost of higher energy consumption. During acquisition, both the probability of frame error P_{fe} and the probability of successful detection P_{det} of a list synchronizer increase with longer list length of the list synchronizer. However, while a higher P_{det} would lead to lower energy consumption, a higher P_{fe} indicates worse receiver performance.

Fig. 2 shows the proposed receiver structure for the new broadcast format. In addition to the demodulation operation, the frequency down-conversion operation is also performed in the digital domain, thus minimizing the complexity of the analog front-end. This operation down-converts the 60 kHz digitized received signal to near baseband, while introducing a frequency offset that corresponds to the frequency inaccuracy of the digital LO signal, which is derived from the receiver's crystal. The implementation complexity of this digital mixing operation is low since the carrier frequency is relatively low. Due to the large relative frequency error of the digital LO and the potentially low SNR conditions, a joint timing, frequency and phase offset estimation is performed. The estimated frequency and phase offsets are used in a second down-conversion operation to down-convert the received signal from up to a few Hz to baseband. A subsequent tracking or acquisition operation is performed on this baseband signal.

II. JOINT FRAME AND SYMBOL SYNCHRONIZATION WITH LARGE FREQUENCY OFFSET

Commercial RCC devices may use a crystal having a frequency inaccuracy of 20 ppm, which will result in a maximum frequency offset of $\Delta f = 1.2$ Hz with respect to the 60 kHz carrier. Due to the long symbol duration of the WWVB broadcast,

the maximum relative frequency offset is $\Delta f = 1.2 \frac{1}{T}$, where T represents the symbol duration of one second. Moreover, this frequency error could further increase with temperature changes. Compared with the large frequency offset assumed in most frequency estimation algorithms [4]–[11], the frequency offset addressed in this paper is much greater and hence it is considered a very large frequency error. Consequently, at the RCC receiver, symbol timing recovery and frame synchronization are performed in the presence of unknown and very large frequency offset, while often also experiencing very low SNR conditions. Therefore, it is desirable to perform a data-aided joint symbol and frame synchronization operation, such that the timing decision is made by exploiting the entire known synchronization word, resulting in higher effective output SNR than the received SNR per symbol.

Frame synchronization in the presence of frequency offset has been studied in [4]–[11]. It is assumed in [4]–[8] that the frequency offset is a fraction of the symbol rate, which accurately models high data rate systems. To deal with large frequency errors, post-detection integration (PDI) techniques are used, based on a combination of coherent and non-coherent operations [9]–[11]. The coherent integration time is determined such that the cumulative phase error is tolerable (e.g., below $\pi/2$). In the WWVB receivers, such coherent integration interval is shorter than the symbol duration due to the very large frequency offset. This results in a correspondingly low amount of accumulated signal energy, requiring the SNR to be sufficiently high (about 10 dB). In contrast, the tracking mode, designed to operate at lower SNR, is based on the detection of a sync word, which extends over 14 symbol durations. This longer integration duration requires the frequency offset to be reduced to within a fraction of the symbol rate.

This paper proposes two joint symbol and frame synchronization schemes that operate in the presence of very large frequency offsets, one based on maximum likelihood (ML) criteria and the other based on correlation. Since analytical performance evaluation is intractable, Monte Carlo simulations are used to assess the performance of the synchronizer.

A. Synchronization Problem Formulation

In Normal mode, the transmitted signal, $x(t)$, at time t can be written as:

$$x(t) = \sum_{n=-\infty}^{\infty} e^{j\theta_n} g_n(t - nT + t_d) e^{j2\pi f_c t} \tag{1}$$

where f_c is the carrier frequency. The phase θ_n is determined by the nth PM symbol, where binary "0" and "1" correspond, respectively, to $\theta_n = 0$ and π. In a Normal 60-second time-code frame of the enhanced broadcast, the first 13 and the last PM symbols of each frame are fixed, corresponding to the predefined 14-bit sync word [3]. The length of this sync word and the duration of the frame are denoted, respectively, by l_{sw} and l_f. The rest of the frame is populated with data corresponding to the time information, which is to be considered random. The pulse shape $g_n(t - nT + t_d)$ is determined by the nth AM/PWM symbol, shown in Fig. 1. There is a delay of 100 ms, denoted t_d, from the start of each AM bit before the
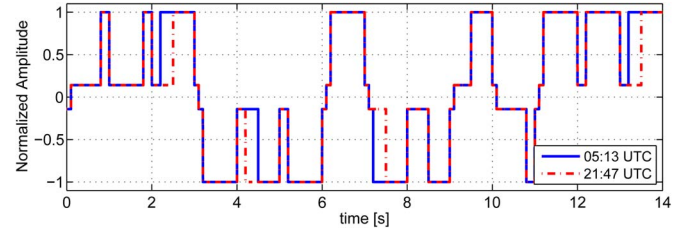

Fig. 3. Two examples of sync word waveforms transmitted at different times. The PM bits are 00011101101000 for both examples, and the AM/PWM bits are MM00100011M000 and MM10000111M001 respectively, where M denotes marker bits.

phase changes based on the transmitted PM bits [12]. This delay serves to decrease the abrupt changes in the signal, thereby concentrating its spectral energy around the carrier to minimize the power reflected from the station's narrowband antenna. As shown by the two examples in Fig. 3, the 14 PM bits of the sync word are predefined, while the AM bits overlapping with them correspond to the time information and may vary.

Receivers in acquisition operation, for which the frame timing is unknown, use a reception duration of $l_{rx} = 2l_f$, during which the signal is digitally recorded, in order to obtain a complete coded frame. For receivers in tracking operation, for which the frame timing is known to within t_s, the receive duration that can guarantee the capture of a continuous sync word is $l_{rx} = l_{sw} + 2t_s$, where t_s denotes the timing search interval at the receiver.

At the receiver, the start of reception is at time $t = 0$ and the next closest start of a frame (SOF) is at time $t = \mu$. The frequency and phase offsets are denoted by Δf and ϕ_0, respectively. The sampling rate, N, at the output of the LPF (low-pass filter) and down-sampling block should be higher than $2(B + \max(\Delta f))$, where B is the signal bandwidth and $\max(\Delta f)$ is the maximum frequency offset that the receiver's LO may experience (typically determined by the accuracy of the receiver's crystal). Let $T_s = \frac{1}{N}$ denote the sampling duration. We assume T_s is small enough such that the phase offset due to the residual timing between μ and its nearest sampling instance mT_s is included in the phase offset ϕ_0. Therefore, we have $\mu \approx mT_s$. The total number of receive samples is $N_{rx} = Nl_{rx}$. Let $\mathbf{r} = (r_0, r_1, \ldots, r_{N_{rx}-1})$ denote the received samples at the output of the LPF and downsampling, in which there are non-baseband (due to frequency offset) and noise corrupted sync word samples $\mathbf{c} = (c_0, c_1, \ldots, c_{Nl_{sw}-1})$ and data samples $\mathbf{d} = \{d_k, \forall k \notin \psi_m\}$. Set $\psi_m = \{m, m+1, \ldots, m + Nl_{sw} - 1\}$ denotes the indices of the sync word samples given that the SOF is at instance m. Since the propagation conditions of the 60 kHz WWVB signal vary slowly and can be considered fixed throughout a reception operation, we assume a simple additive white Gaussian noise (AWGN) channel in the simulations. The kth received signal, r_k, can be written as:

$$r_k = \begin{cases} c_{k-m} e^{j(2\pi\Delta f(k-m)T_s + \phi_0)} + z_k & \text{if } k \in \psi_m \\ d_k e^{j(2\pi\Delta f(k-m)T_s + \phi_0)} + z_k & \text{if } k \notin \psi_m \end{cases} \tag{2}$$

where z_k is a zero-mean complex white Gaussian noise with the variance $\sigma_z^2 = \frac{N_0}{2T_s}$. The goal of the synchronization operation is to estimate m given the received signal $\mathbf{r}$. The set of possible values of timing estimate $\hat{m} \in \mathbb{M}_a = \{0, 1, \ldots, Nl_f - 1\}$ for acquisition and $\hat{m} \in \mathbb{M}_t = \{0, 1, \ldots, 2\lceil Nt_s \rceil\}$ for tracking.

B. ML Synchronization Algorithm

Using the Maximum Likelihood (ML) criteria, the desired timing, frequency and phase offset maximize the conditional probability density function (PDF) $p(r|m, \Delta f, \phi_0, \mathbf{d}, \mathbf{c})$ of received signal r given by (3), shown at the bottom of the page, where $d_l^{(i)}$ is the l-th sample of the i-th random data symbol with envelope $|d_l^{(i)}|$ determined by the AM bits, and phase $\angle d^{(i)}$ determined by the PM bits. Similarly, c_k is the k-th sample of the sync word with envelope $|c_k|$ determined by the AM bits, and predetermined phase $\angle c_k$ corresponding to the sync word. Constant $A = \left(\frac{T_s}{\pi N_0}\right)^{N_{rx}} \prod_{k=0}^{N_{rx}-1} e^{-|r_k|^2 \frac{T_s}{N_0}}$ is not dependent on m, Δf, ϕ_0, $\mathbf{d}$, and $\mathbf{c}$. The indexes of sync word symbols given SOF at time m is denoted by Ψ_m, and the set of samples that belongs to symbol i is denoted by γ_i.

During acquisition, the AM bits are unknown and the probabilities of the i-th bit being "0" and "1" are denoted by $p_i^{(0)}$ and $p_i^{(1)} = 1 - p_i^{(0)}$, respectively. Averaging the conditional PDF over all possible amplitude of received symbols $\mathbf{c}$ and $\mathbf{d}$, we get (4), shown at the bottom of the page, where $q^{(j)}$ is the probability of the j-th sync word waveform $\mathbf{c}^{[j]}$, and $j = 0, 1, \ldots 2^8 - 1$ since there are 8 unknown AM bits during acquisition of the sync word in the PM broadcast [3]. The l-th sample of the amplitude envelope of AM "0" and "1" are denoted by $|d_l^{[0]}|$ and $|d_l^{[1]}|$ respectively. The computation of (4) requires approximately $1.8 \times 10^4 N$ multiplications and $1.1 \times 10^4 N$ additions, where $N \geq 10$ when assuming the maximum frequency offset is 4 Hz and signal bandwidth is 1 Hz. Such implementation complexity is unaffordable for most applications. Therefore, by approximating the amplitude of the unknown AM bits by the average amplitude, we simplify the likelihood function to:

$$p(r|m, \Delta f, \phi_0, \angle\mathbf{d}, \angle\mathbf{c})$$
$$\approx A \prod_{k=0}^{Nl_{sw}-1} e^{\frac{2T_s}{N_0} \mathbb{R}\{\bar{c}_k r_{k+m} e^{-j(2\pi\Delta f k T_s + \phi_0)}\}}$$
$$\times \prod_{i \notin \Psi_m} e^{\frac{2T_s}{N_0} \mathbb{R}\{\sum_{l \in \gamma_i} |\bar{d}_l| |r_{iN+l}| e^{-j(2\pi\Delta f(iN+l-m)T_s + \phi_0 - \angle d^{(i)})}\}} \quad (5)$$
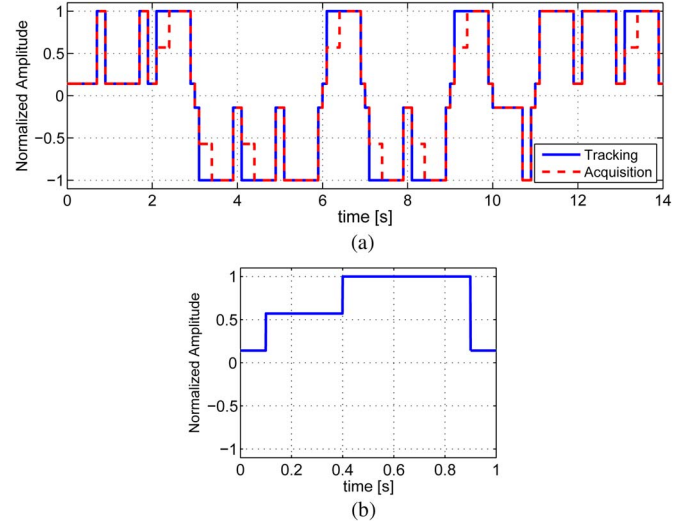

Fig. 4. Receiver locally generated baseband waveform of sync word and baseband envelope of random data. (a) Receiver locally generated baseband waveform of sync word $\bar{\mathbf{c}}$ in tracking and in acquisition; (b) receiver locally generated average baseband envelope of a data symbol $|\bar{\mathbf{d}}|$ for both tracking and acquisition.

where $\bar{\mathbf{c}} = \mathbf{c}$ for tracking at the recommended time [3], and $\bar{\mathbf{c}} = \frac{1}{2^8} \sum_{j=0}^{2^8-1} \mathbf{c}^{[j]}$ for acquisition, as shown by Fig. 4(a). Similarly, $|\bar{\mathbf{d}}| = \frac{1}{2}(|\mathbf{d}^{[0]}| + |\mathbf{d}^{[1]}|)$ for both tracking and acquisition, as shown in Fig. 4(b). Since the average waveform is highly correlated with the actual waveforms of "0" and "1" in AM, with normalized correlation of 0.97 and 0.95 respectively, this approximation results in negligible SNR degradation, which is quantified in Appendix A. However, the implementation complexity required to compute (5) is reduced significantly especially in acquisition, since the number of multiplications and additions are only about $180N$ and $120N$ respectively. Note that implementation complexity is used broadly to refer to the number of multiplications and additions.

Since BPSK modulation implies that $\angle d^{(i)}$ is $-\pi$ or π with equal probability, averaging the conditional PDF over all possible phases of random data $\mathbf{d}$, using the approximation of

---

$$p(r|m, \Delta f, \phi_0, \mathbf{d}, \mathbf{c}) = A \prod_{k=m}^{m+Nl_{sw}-1} e^{-\frac{T_s}{N_0}\left(|c_{k-m}|^2 - 2\mathbb{R}\{c_{k-m} r_k e^{-j(2\pi\Delta f(k-m)T_s + \phi_0)}\}\right)}$$
$$\times \prod_{i \notin \Psi_m} \prod_{l \in \gamma_i} e^{-\frac{T_s}{N_0}\left(\left|d_l^{(i)}\right|^2 - 2\mathbb{R}\left\{\left|d_l^{(i)}\right| |r_{iN+l}| e^{-j\left(2\pi\Delta f(iN+l-m)T_s + \phi_0 - \angle d^{(i)}\right)}\right\}\right)} \quad (3)$$

$$p_{acq}(r|m, \Delta f, \phi_0, \angle\mathbf{d}, \angle\mathbf{c}) = A \prod_{k=0}^{Nl_{sw}-1} \sum_{j=0}^{2^8-1} q^{(j)} e^{-\frac{T_s}{N_0}\left(|c_k^{[j]}|^2 - 2\mathbb{R}\{c_k^{[j]} r_{k+m} e^{-j(2\pi\Delta f k T_s + \phi_0)}\}\right)}$$
$$\times \prod_{i \notin \Psi_m} \prod_{l \in \gamma_i} \sum_{j=0}^{1} p_i^{(j)} e^{-\frac{T_s}{N_0}\left(|d_l^{[j]}|^2 - 2\mathbb{R}\{|d_l^{[j]}| |r_{iN+l}| e^{-j(2\pi\Delta f(iN+l-m)T_s + \phi_0 - \angle d^{(i)})}\}\right)} \quad (4)$$

$\cosh(y) \approx \frac{1}{2}e^{|y|}$ and dropping the constants, the log-likelihood function (LLF) $\Lambda_{BPSK}(r|m, \Delta f, \phi_0, \angle\mathbf{c})$ is:

$$\Lambda_{BPSK}(r|m, \Delta f, \phi_0, \angle\mathbf{c})$$
$$= \sum_{k=0}^{Nl_{sw}-1} \mathbb{R}\left\{\bar{c}_k r_{k+m} e^{-j(2\pi\Delta fkT_s + \phi_0)}\right\}$$
$$+ \sum_{i \notin \Psi_m} \left| \mathbb{R}\left\{ \sum_{l \in \gamma_i} |\bar{d}_l| r_{iN+l} e^{-j(2\pi\Delta f(iN+l-m)T_s + \phi_0)} \right\} \right| \quad (6)$$

However, there is no direct-form solution for phase ϕ_0 that can maximize the sum of both terms in (6). We prove in Appendix C that the Cramér-Rao Bound (CRB) of phase estimate derived from the sync word portion (first term in (6)) is lower than that derived from the random data portion (second term in (6)). Therefore, in this paper, the phase estimate $\hat{\phi}_0$ that maximizes the first term in (6) is used and is given by:

$$\hat{\phi}_0(m, \Delta f) = \arctan\left\{ \sum_{k=0}^{Nl_{sw}-1} \bar{c}_k r_{k+m} e^{-j2\pi\Delta fkT_s} \right\} \quad (7)$$

Substituting (7) into (6), we get:

$$\Lambda_{BPSK}(r|m, \Delta f, \angle\mathbf{c})$$
$$= \left| \sum_{k=0}^{Nl_{sw}-1} \bar{c}_k r_{k+m} e^{-j2\pi\Delta fkT_s} \right|$$
$$+ \sum_{i \notin \Psi_m} \left| \mathbb{R}\left\{ \sum_{l \in \gamma_i} |\bar{d}_l| r_{iN+l} e^{-j\left(2\pi\Delta f(iN+l-m)T_s + \hat{\phi}_0(m, \Delta f)\right)} \right\} \right|$$
$$= \Lambda_s(r|m, \Delta f, \angle\mathbf{c}) + \Lambda_d(r|m, \Delta f) \quad (8)$$

Note that the first term in (8) is the correlation between the received signal and the locally generated waveform, and the second term is called the random data correction [13]. Similar to (6), no closed form solution for Δf that maximizes (8) is known. In Appendix C, we also prove that the CRB for the frequency estimate derived from the sync word portion Λ_s is lower than that derived from the random data portion Λ_d. Therefore, in this paper the frequency estimation is based on the sync word only, given by:

$$\Delta\hat{f}(m) = \arg\max_{\Delta f} \Lambda_s(r|m, \Delta f, \angle\mathbf{c}) \quad (9)$$

The optimal solution of (9) can be obtained using a fast Fourier transform (FFT) [14]. There also exist low-complexity approaches of frequency estimation [15]–[17] that can provide a large enough frequency estimation range and low enough SNR threshold for RCC devices, where SNR threshold refers to the SNR value above which the frequency estimator can achieve the CRB.

After obtaining the frequency estimate $\Delta\hat{f}(m)$ for a given timing m using existing frequency estimation approaches, the ML-BPSK timing estimate is obtained by:

$$\hat{m}_{ML-BPSK} = \arg\max_m \Lambda_{BPSK}(r|m, \Delta\hat{f}(m), \angle\mathbf{c}) \quad (10)$$

However, the calculation of $\Lambda_{BPSK}(r|m, \Delta\hat{f}(m), \angle\mathbf{c})$ requires the computation of $\hat{\phi}_0(m, \Delta f)$, which involves a further look-up table for the arctan function. Since the phase of the BPSK modulated random data $\angle d^{(i)}$ is coupled with an unknown phase error ϕ_0, to further simplify the implementation we assume $\angle d^{(i)}$ is uniformly distributed over $(-\pi, \pi]$ (continuous phase modulation or CPM). Note that this assumption is only used to simplify the synchronization algorithm, and the actual recovery of data that is implemented later in acquisition operation still observes BPSK demodulation rules. Starting from (5) and using the approximation of $I_0(x) \approx e^{|x|}/\sqrt{2\pi}$, where $I_0(x)$ is the zeroth-order modified Bessel function, the CPM based ML timing estimate, $\hat{m}_{ML-CPM}$, is given by:

$$\hat{m}_{ML-CPM} = \arg\max_m \Lambda_{CPM}(r|m, \Delta\hat{f}(m), \angle\mathbf{c}) \quad (11)$$

where

$$\Lambda_{CPM}(r|m, \Delta f, \angle\mathbf{c})$$
$$= \left| \sum_{k=0}^{Nl_{sw}-1} \bar{c}_k r_{k+m} e^{-j2\pi\Delta fkT_s} \right|$$
$$+ \sum_{i \notin \Psi_m} \left| \sum_{l \in \gamma_i} |\bar{d}_l| r_{iN+l} e^{-j2\pi\Delta flT_s} \right|$$
$$= \Lambda_s(r|m, \Delta f, \angle\mathbf{c}) + \Lambda'_d(r|m, \Delta f) \quad (12)$$

The correlation based timing estimate, $\hat{m}_{corr}$, is obtained by only considering Λ_s in (12), and is given by:

$$\hat{m}_{corr} = \arg\max_m \Lambda_s(r|m, \Delta\hat{f}(m), \angle\mathbf{c}) \quad (13)$$

It requires $7Nl_c$ multiplications and $3Nl_c$ additions to compute the LLF, where the l_c is the length of received signal considered in the LLF and $l_c = l_{rx}$ for Λ_{CPM} and $l_c = l_{sw}$ for Λ_s. Therefore, the computational complexity of the correlation based approach is only about 23% and 50% of the ML based approaches in acquisition and tracking, respectively. The proposed algorithm for joint symbol and frame synchronization is summarized as follows:

- For every timing m in set $\mathbb{M}$, compute $\Delta\hat{f}(m)$ in (9) using existing frequency estimation algorithms.
- Substitute $\Delta\hat{f}(m)$ to compute metrics Λ_{BPSK}, Λ_{CPM}, or Λ_s for ML-BPSK, ML-CPM and correlation based algorithms respectively.
- After calculating the metrics Λ_{BPSK}, Λ_{CPM}, or Λ_s for all timings in set $\mathbb{M}$, choose the timing that maximizes the desired metric.

C. Performance of Various Timing and Frequency Estimation Approaches

The simulation assumes the use of a 20 ppm local crystal that satisfies the three-sigma rule, i.e., 99.73% of the crystals can provide 20 ppm frequency tolerance at 25 °C. By also taking into account the frequency drift within a standard operating temperature range −10 °C to 60 °C, the maximum frequency offset $\max(\Delta f) = 4$ Hz. Note that we assume the crystal's
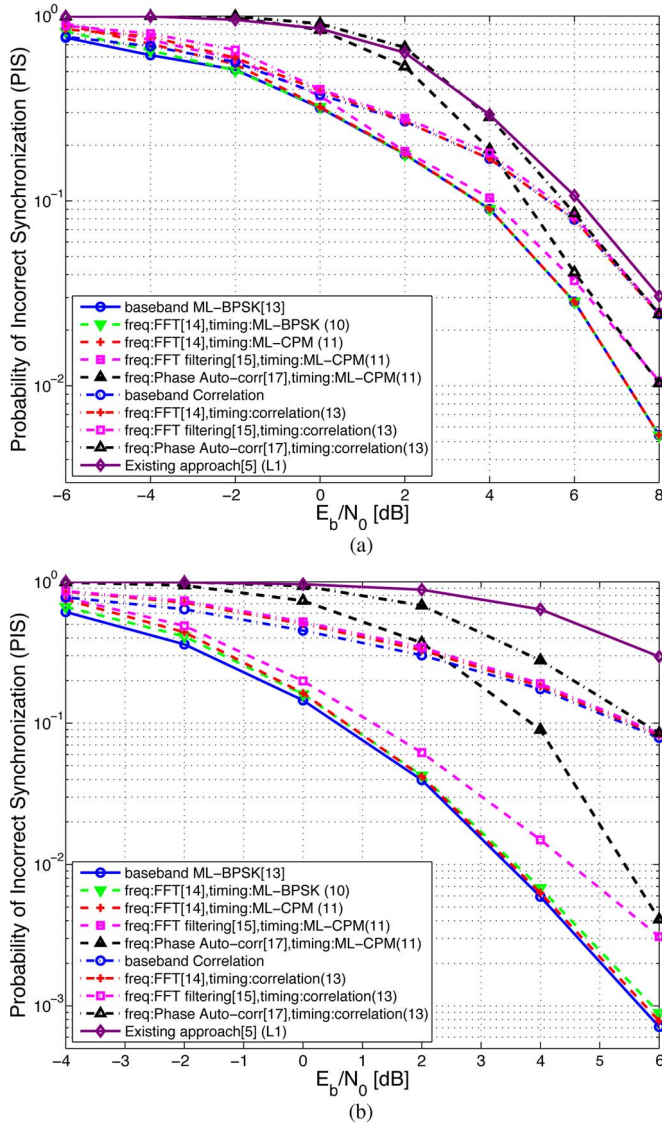
Fig. 5. Probability of incorrect synchronization at the output of the synchronizer using different frequency and timing estimation approaches. Frequency estimation approaches include FFT, FFT filtering and auto-correlation. Timing estimation approaches include, ML-BPSK (10), ML-CPM (11) and correlation (13). Two bounds are also given for comparison. The baseband ML-BPSK approach offers a lower bound for the ML-BPSK and ML-CPM approaches, and the baseband correlation approach offers a lower bound for correlation based approaches. The performance of an existing approach in [5] is also shown for comparison. (a) Tracking scenario; (b) acquisition scenario.

parabolic coefficient K_1 is 4×10^{-8} [18]. Since tracking is assumed to perform daily, we assume the time error of the local crystal is normally distributed with variance $\sigma_t^2 = 4 \text{ s}^2$ within the maximum timing offset $\max(\Delta t) = 6$ s. In tracking, to prevent the timing drift from exceeding the receiver's timing search interval t_s, t_s should equal the maximum timing offset, i.e., $t_s = \max(\Delta t) = 6$ s. For acquisition, the timing search interval $t_s = 30$ s. The time information represented by the transmitted signal is randomly chosen among all the possible dates in this century for acquisition, and among all the possible dates in this century at the default tracking time for tracking [3]. The oversampling rate at the receiver is $N = 20$.

Fig. 5 shows the probability of incorrect synchronization (PIS) using different timing and frequency estimation ap-

proaches during tracking and acquisition. PIS is defined as the probability that the estimated timing $\hat{m} \neq m$. Also shown in Fig. 5 is the PIS for the baseband ML-BPSK synchronization [13] and correlation based synchronization approaches, i.e., with known frequency and phase, providing a lower bound for PIS using all three timing estimation approaches: ML-BPSK, ML-CPM and correlation. Clearly, the ML-BPSK and ML-CPM approaches exhibit performance close to that of the ML approach with known frequency and phase, indicating the phase estimates in (7) and frequency estimates in (9) provide near-optimal performance. Compared with the correlation based approaches, the ML approaches yield smaller PIS, especially during acquisition, due to the larger number of random data symbols used in the computation. For the same reason, the PIS is smaller in acquisition than in tracking for the ML approaches. By contrast, with the same number of symbols taken into account, the correlation based estimates have a smaller PIS in tracking than in acquisition, as a result of the narrower timing search range in tracking. The performance of an existing synchronization approach in [5], which can address relatively large frequency offset, is also shown for comparison. Since the maximum frequency offset at the receiver is larger than the estimation range of the existing approaches, the performance of the existing approach is worse than that of the proposed approaches in both tracking and acquisition.

Fig. 5 also compares the performance of three frequency estimation approaches: 8192-point FFT, FFT filtering with $L = 140$ [15] and auto-correlation with $N = 140$ [17]. In both tracking and acquisition, the FFT filtering approach introduces SNR degradation of about 1 dB compared with the optimal FFT approach, while significantly reducing the computational complexity [15]. Therefore, the FFT filtering approach is used for frequency estimation during synchronization.

III. DECISION STRATEGIES FOR THE TRACKING OPERATION

Since the purpose of the tracking operation is to correct the timing error due to the inaccuracy of the local crystal, the MSE of the estimated timing is selected as the performance metric for tracking. In this section, we first present the trade-off between performance and energy consumption by varying receiver parameter t_s. Then we study the performance improvements obtained using two different decision strategies: an optimal minimum mean square error (MMSE) approach (soft tracking) and a low complexity approach (hard tracking).

A. MSE Performance at the Output of Synchronization

Fig. 6 shows the MSE of the timing estimation at the output of the synchronization operation, with ML-CPM and correlation approaches based on the new PM broadcast, and envelope detection based on the legacy AM broadcast. The simulation parameters are identical to those in Section II-C for tracking. As in the case of most conventional RCC devices, we assume envelope detection uses a crystal filter with 10 Hz bandwidth to filter the received RF signal [12]. It is to be noted that typical envelope-detection based receivers for the legacy
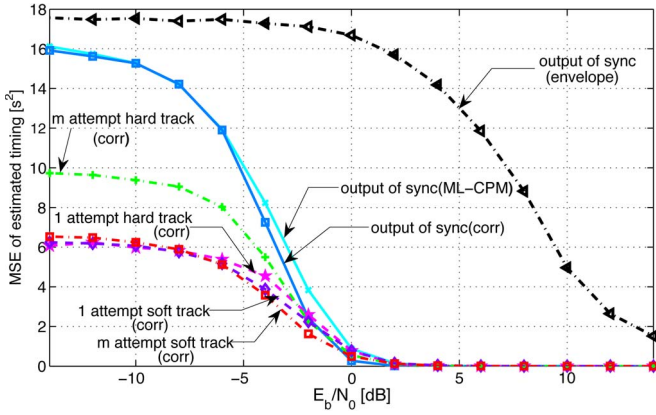
Fig. 6. MSE of estimated timing at the output of the synchronizer (without additional processing) and at the output of the tracking decision (with two different decision strategies).

broadcast neither employ a tracking operation based on correlation against multiple known bits nor implement a decoded-assisted acquisition. The comparison in Sections III and IV are therefore theoretical, and the performance of conventional receivers based on the legacy format is, in practice, inferior to what is assumed in the comparisons.

In Fig. 6, the synchronization based on the PM broadcast is shown to be about 15 dB better than that based on the legacy broadcast at higher SNR, from which 12 dB performance gain is provided by the improved modulation and 3 dB performance gain is provided by the synchronization algorithm. Besides, the performance gap becomes marginal between the two PM broadcast based synchronization approaches: correlation and ML-CPM, because the random data correction term Λ_d or Λ'_d in the ML criteria improves the symbol timing more than the frame timing. While the PIS in Fig. 5 treats the errors in symbol and frame timing equally, the MSE is dominated by errors in frame timing since their squared error is quantitatively larger. In light of the marginal performance difference between the ML approach and correlation based approach, the correlation approach is used for subsequent analysis in tracking.

It is important to select an appropriate timing search interval t_s. The longer the timing search interval, the higher the computational and reception energy consumption. The correlation based synchronizer requires $2\lceil Nt_s \rceil$ length-140N FFTs and $28N\lceil Nt_s \rceil$ complex multiplications. Further, the receive duration for tracking is $l_{sw} + 2t_s$. Consequently, although it guarantees to search all possible timing errors by setting $t_s = \max(\Delta t)$, a smaller t_s can reduce the complexity at the risk of timing drift exceeding t_s. Such risk can be reduced after studying several tracking operations. For example, if several reliable tracking operations indicate the timing drifts fall into a narrower range, t_s can be reduced accordingly.

B. MMSE Approach: Tracking With Soft Decision

In addition to the estimated timing $\hat{m}$, derived from the received WWVB signal, RCC devices have a local crystal that can provide an independent timing estimate, m_c. Therefore, the minimum MSE algorithm applies a MMSE filter $\bar{w} = [a, 1-a]^{\mathrm{T}}$ to the two timing estimates $\bar{t} = [\hat{m}, m_c]^{\mathrm{T}}$, to obtain the timing es-

timate $m_{MMSE} = \bar{w}^{\mathrm{T}}\bar{t}$. By making the high SNR approximation $E[\mu^2] \approx E[\mu\hat{m}]$, it is easy to derive the filter coefficient a which minimizes the MSE between μ and m_{MMSE}, as:

$$a(\rho) = \frac{\sigma_t^2}{\sigma_e^2(\rho) + \sigma_t^2} \tag{14}$$

where $\sigma_e^2(\rho)$ denotes the MSE of $\hat{m}$ at the output of the synchronizer at SNR ρ, and $\sigma_e^2(\rho)$ is given by Fig. 6. The value of $\sigma_e^2(\rho)$ can be obtained by using a look-up table in the receiver implementation, and simulations shown in Section III-D use a look-up table with 401 8-bit entries, representing $\sigma_e^2(\rho)$ for -10 dB $\leq \rho \leq 10$ dB. The weight a monotonically increases from 0 to 1 as SNR increases, with $\sigma_e^2(-10\text{dB}) \approx 0$ and $\sigma_e^2(10 \text{ dB}) \approx 1$. Therefore, any values of $\rho < -10$ dB and $\rho > 10$ dB are truncated to -10 dB and 10 dB, respectively, in the look-up table. Since it is impractical for the receiver to have perfect SNR knowledge, in reality, the estimated SNR $\hat{\rho}$ is used in (14) to derive the optimal filter coefficient. Since the weight a is in the range $0 < a < 1$, we call this MMSE algorithm *soft tracking*.

In reality, SNR could vary with time due to changes in the environment, such as a changing level of interference or reception signal strength. Therefore, for RCC devices that can afford higher energy consumption, it is possible to encounter a higher SNR with repeated receptions, thus increasing the accuracy of the estimate. Given Q attempts are made, the MMSE timing estimate m_{MMSE} is obtained by filtering the $Q+1$ timings, with the first timing m_c based on the local crystal having variance of σ_t^2 and the remaining timing estimates $\hat{m}_i$ derived from the i-th received WWVB signals having variance of $\sigma_e^2(\rho_i)$. Since the summation of all elements of the filter coefficient $\bar{w}$ is one, we rewrite the filter coefficient $\bar{w} = [1 - \sum_{i=1}^{Q} \eta_i, \bar{\eta}^T]$. The length Q optimal MMSE coefficient vector $\bar{\eta}$ is given by:

$$\bar{\eta} = \begin{bmatrix} \sigma_t^2 + \sigma_e^2(\rho_1) & \sigma_t^2 & \cdots & \sigma_t^2 \\ \sigma_t^2 & \sigma_t^2 + \sigma_e^2(\rho_2) & \cdots & \sigma_t^2 \\ \vdots & \vdots & \ddots & \vdots \\ \sigma_t^2 & \sigma_t^2 & \cdots & \sigma_t^2 + \sigma_e^2(\rho_Q) \end{bmatrix}^{-1} \sigma_t^2 \tag{15}$$

where length Q vector $\sigma_t^2 = [\sigma_t^2, \ldots, \sigma_t^2]^{\mathrm{T}}$. The minimum MSE is:

$$E_{min}\left[t_e^2\right] = \sigma_t^2 \left(1 - \sum_{i=1}^{Q} \eta_i\right). \tag{16}$$

The steps in implementing soft tracking based on multiple receptions can be summarized as follows:

- Upon the i-th reception attempt, RCC receivers using soft tracking obtain MMSE timing estimate m_{MMSE} using (15) and the corresponding MSE using (16).
- If the MSE is higher than a certain threshold ξ, an additional reception is attempted; otherwise, reception could stop and the final output timing would be $m = \bar{w}^{\mathrm{T}}\bar{t}$.

In a practical implementation, the maximum number of reception attempts can be limited by Q_{max}, which would consider implementation complexity. In cases where Q_{max} receptions

are insufficient, the receiver can schedule another reception to receive signals of other transmission modes with lower bit rate and longer frame duration [2], [3].

The worst case scenario of multiple receptions is that the SNR does not improve with time for whatever reason, such as persistent interference. Due to the inaccuacy of SNR estimation in low SNRs, it is probable that the inaccurate SNR estimates will degrade the performance. We quantify the performance degradation under the worst case scenario in Section III-D.

C. Tracking With Hard Decision

The proposed soft tracking method requires a look-up table in the receiver that can output the corresponding MSE $\sigma_e^2(\rho)$ given an estimated SNR ρ. A single table look-up operation is required for each reception attempt followed by a filtering step. To reduce the computational complexity, we present a simplified *hard tracking* algorithm where the filter coefficient is either 0 or 1. In other words, the output timing equals the timing estimate provided by the local crystal if the SNR is below a threshold, ρ_t, or accepts the timing estimate derived from the received WWVB signal if the SNR is higher than ρ_t. To minimize the MSE of estimated timing using hard tracking, this SNR threshold ρ_t is chosen such that $\sigma_e^2(\rho_t) = \sigma_t^2$. Similar to soft tracking, multiple attempts could be made to refine the estimated timing in hard tracking.

D. Simulation Results

Fig. 6 compares the performance of hard tracking and soft tracking assuming both single and multiple reception attempts. The scenario of multiple receptions is shown with $Q_{max} = 3$, where the SNR does not change across all reception attempts. In the simulations, the synchronization is based on the correlation approach given by (13), and the ML TXDA SNR estimator [19] is used to obtained the SNR estimates. In case Q_{max} receptions are insufficient, the output timing is the last updated m_{MMSE} for soft tracking and m_c for hard tracking. The MSE threshold is set at $\xi = 1.6$ s^2 for soft tracking, such that the difference in the average number of reception attempts between soft decision and hard decision is within 10% for all SNRs to ensure fair comparison.

The results in Fig. 6 show the following. First, compared with the MSE at the output of the synchronizer, using either hard or soft decision improves the MSE performance in all SNRs. With a single reception, either decision strategy could effectively reduce the variance in the timing error by 63% at low SNRs. It is important to note that a static RCC device that has successfully performed acquisition could still encounter low SNRs during tracking, since interference and MMN vary temporally. Second, since the timing MSE using both decision strategies at low SNR is bound by a value higher than σ_t^2 due to low SNR and resulting inaccuracy in SNR estimation, the tracking operation could improve the accuracy of the RCC only for SNR higher than -4 dB for these simulation parameters. Third, while the performance advantage of soft tracking over hard tracking is marginal assuming single reception, the performance advantage

is significant when multiple receptions are allowed. Finally, when assuming SNR does not change across multiple receptions, the MSE using multiple receptions improves slightly at higher SNR. However, the MSE degrades at consistent low SNRs, especially for hard tracking, due to the inaccuracy in SNR estimation.

IV. DETECTION FOR ACQUISITION OPERATION

The goal of the acquisition operation is to decode the time information for it to be used by the device. Various data fields in the frame are encoded by block codes with different block lengths. Since the initial timing synchronization prior to data decoding is based on an uncoded sync word, the error detection/correction capability for the data fields may serve to enhance the overall robustness of synchronization and data recovery. In this section, the joint synchronization and decoding algorithm is presented, with analysis of the trade-off between performance and energy consumption, as well as performance comparison between the ML approach and correlation approach in synchronization.

A. Prior Work and the Proposed Algorithm

Ideally, optimal decoder-assisted frame synchronization should select the timing such that the joint likelihood function of timing and data is maximized. The complexity of the optimal approach is high since the decoder needs to calculate the likelihood function for all possible timings over all possible codewords. A lower complexity list synchronizer approach [20]–[25] only performs decoding on a list of ν most probable timings. Further, existing decoder-assisted frame synchronization approaches target sophisticated channel codes with higher coding gain, such as convolutional codes [21]–[24], turbo code [25] and LDPC code [26].

In a Normal frame of the WWVB broadcast, the channel code with the strongest error-control capability, the Hamming (31,26) code that is at least 5 times longer than other channel codes used in a frame, can only correct one bit error. Further, since the synchronizer proposed in Section II jointly estimates symbol timing, frame timing, and frequency offset, the computational complexity is usually higher than that found in high data rate systems, where the symbol timing is already obtained and frequency offset is fractional with respect to data rate. Considering the computational complexity and the simplicity of the channel code, unlike [20], [23], and [27], which utilize soft metrics such as LLF and LLR (log-likelihood ratio), we only utilize the syndrome of the received Hamming (31,26) code. To further reduce the complexity, the proposed joint synchronization and decoding algorithm is based on a list synchronization operation. The analysis is, however, different from prior works [20]–[25], since the receiver has the option of discarding the acquisition result and making a second attempt upon unreliable reception.

The proposed joint synchronization and decoding algorithm is described as follows:

- The synchronizer outputs a list of ν most probable timing offsets to the Hamming decoder.

- The decoder performs syndrome decoding for each timing offset given by the list in the order of most probable timing offset to least probable timing offset.
- For the i-th timing on the list, the decoder would declare a detection if the syndrome is zero for the given timing. In this case, a *frame error* occurs if the decoded message is different from the transmitted message, and a *successful detection* occurs if the decoded message is identical to the transmitted message. If the syndrome of the i-th timing is non-zero, the decoder will proceed to the $(i+1)$-th timing on the list.
- The receiver will discard the acquisition result if no timing on the list provides zero syndrome in the decoder, and this is called an *erasure* event. A second reception attempt may be made in this case.

The most important parameter in the proposed algorithm is the list length ν, and it is important to study the effect of list length on the performance of the receiver. The performance metrics used are the probability of frame error P_{fe} and the probability of successful detection P_{det}. The probability of erasure is $P_{era} = 1 - P_{fe} - P_{det}$. Let M denote the event of *missed list*, i.e., the correct timing m is not in the list. The probability of missed list for length-ν list is denoted as $P_M(\nu)$. In contrast, $P_{\bar{M},\alpha}(\nu)$ denotes the probability that the correct timing m is the α-th entry of the list. Clearly, $P_M(\nu) + \sum_{\alpha=1}^{\nu} P_{\bar{M},\alpha}(\nu) = 1$. Given the correct timing m, the probability that one or more bit errors occur in the n-bit frame is denoted as P_{EC}, and the probability of undetected error in the Hamming code is denoted as P_{UE}. Given any incorrect timing $\tau \neq m$, the probability that the corresponding received signal gives zero syndrome but incorrect decoded message is $P_R(\tau)$, and the probability that the corresponding received signal gives zero syndrome and correct decoded message is $P_L(\tau)$. The probability of event X occurring with length-ν list, $P_X(\nu)$, is given by:

$$P_X(\nu) = P_M(\nu) P_{X|M}(\nu) + \sum_{\alpha=1}^{\nu} P_{\bar{M},\alpha}(\nu) P_{X|\bar{M},\alpha}(\nu) \quad (17)$$

where event $X = \{det, fe, era\}$. Let us denote the list of timings as $[\tau_1, \tau_2, \ldots, \tau_\nu]$. The conditional probabilities, $P_{det|M}(\nu)$ and $P_{det|\bar{M},\alpha}(\nu)$ are given by:

$$
\begin{aligned}
&P_{det|M}(\nu)\\
&= P_L(\tau_1) + (1 - P_R(\tau_1) - P_L(\tau_1)) P_L(\tau_2) + \ldots \\
&\quad + \prod_{i=1}^{\nu-1} (1 - P_R(\tau_i) - P_L(\tau_i)) P_L(\tau_\nu), \text{ and}
\end{aligned}
$$

$$
\begin{aligned}
&P_{det|\bar{M},\alpha}(\nu)\\
&= P_L(\tau_1) + (1 - P_R(\tau_1) - P_L(\tau_1)) P_L(\tau_2) \\
&\quad + \ldots + \prod_{i=1}^{\alpha-1} (1 - P_R(\tau_i) - P_L(\tau_i)) (1 - P_{EC}) \\
&\quad + \prod_{i=1}^{\alpha-1} (1 - P_R(\tau_i) - P_L(\tau_i)) (P_{EC} - P_{UE}) P_L(\tau_{\alpha+1}) \\
&\quad + \ldots + \prod_{\substack{i=1\\i\neq\alpha}}^{\nu-1} (1 - P_R(\tau_i) - P_L(\tau_i)) (P_{EC} - P_{UE}) P_L(\tau_\nu).
\end{aligned}
$$

$$(18)$$

Similarly, the conditional probabilities $P_{fe|M}(\nu)$, $P_{fe|\bar{M},\alpha}(\nu)$, $P_{era|M}(\nu)$, and $P_{era|\bar{M},\alpha}(\nu)$ are given respectively by,

$$
\begin{aligned}
&P_{fe|M}(\nu)\\
&= P_R(\tau_1) + (1 - P_R(\tau_1) - P_L(\tau_1)) P_R(\tau_2) + \ldots \\
&\quad + \prod_{i=1}^{\nu-1} (1 - P_R(\tau_i) - P_L(\tau_i)) P_R(\tau_\nu), \text{ and}
\end{aligned}
$$

$$
\begin{aligned}
&P_{fe|\bar{M},\alpha}(\nu)\\
&= P_R(\tau_1) + (1 - P_R(\tau_1) - P_L(\tau_1)) P_R(\tau_2) + \ldots \\
&\quad + \prod_{i=1}^{\alpha-1} (1 - P_R(\tau_i) - P_L(\tau_i)) P_{UE} \\
&\quad + \prod_{i=1}^{\alpha-1} (1 - P_R(\tau_i) - P_L(\tau_i)) (P_{EC} - P_{UE}) P_R(\tau_{\alpha+1}) \\
&\quad + \ldots + \prod_{\substack{i=1\\i\neq\alpha}}^{\nu-1} (1 - P_R(\tau_i) - P_L(\tau_i)) (P_{EC} - P_{UE}) P_R(\tau_\nu),
\end{aligned}
$$

$$(19)$$

$$P_{era|M}(\nu) = \prod_{i=1}^{\nu} (1 - P_R(\tau_i) - P_L(\tau_i)), \text{ and}$$

$$P_{era|\bar{M},\alpha}(\nu) = \prod_{\substack{i=1\\i\neq\alpha}}^{\nu-1} (1 - P_R(\tau_i) - P_L(\tau_i)) (P_{EC} - P_{UE}).$$

$$(20)$$

It is shown in Appendix B and also verified by simulation results that unlike the list synchronizer in [20], both the probability of successful detection and frame error increase with the list length ν with the proposed detection approach. While the probability of frame error P_{fe} indicates the probability that a device would show a wrong time, the probability P_{det} affects the energy consumption of the device, because the average number of reception attempts is $1/P_{det}$ (mean of geometric distribution), assuming the receiver keeps attempting to acquire in Normal mode until a successful detection occurs. Therefore, the choice of list length ν should provide a P_{fe} that is low enough to satisfy the performance requirement of the application, as well as a P_{det} that is high enough to satisfy the energy consumption constraints. The selection of list length should also consider the resulting computational complexity.

B. Simulation Results

Since the analytical expressions for $P_R(\tau)$, $P_L(\tau)$, $P_M(\nu)$, and $P_{\bar{M},\alpha}(\nu)$ are intractable, simulations are used to quantify the tradeoff between the probability of successful detection and the probability of frame error by varying the list length ν for different values of E_b/N_0. The conventional receiver based on envelope detection is also simulated for comparison, where the synchronization result is accepted if the decoded minute is no more than 59, the decoded hour is no more than 23, the decoded day is no more than 365/366, the decoded year is no more than 99, and the decoded year is consistent with the leap year indication. The simulation parameters are the same as those for acquisition in Section II-C. For a particular approach and a particular SNR, the four data points correspond to list lengths 1, 2, 3, and 4.
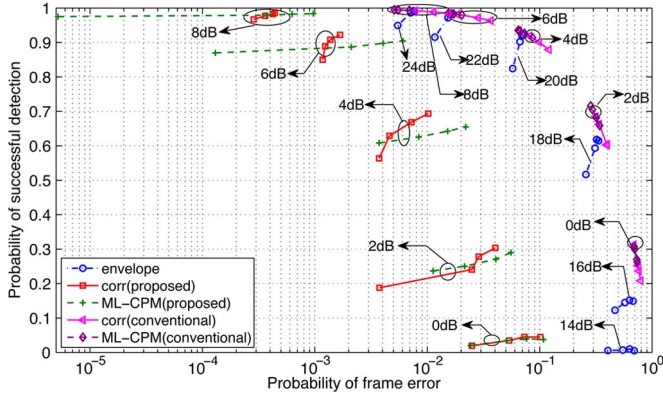
Fig. 7. Probability of successful detection versus probability of frame error using different list length ν.

As shown in Fig. 7, the performance of the proposed joint synchronization and decoding scheme is over 16 dB superior to that of envelope detection based scheme. While the improved modulation offers 12 dB performance gain, the remaining 4 dB performance gain is provided by the acquisition algorithm. It is interesting to note that the correlation criteria achieves higher probability of successful detection with lower probability of frame error for longer list length ($\nu > 1$) at SNR ranging from 2 to 6 dB. This improvement is the result of improved symbol timing brought by the random data correction term Λ'_d or Λ_d. When multiple timings are allowed in the list, the ML-CPM approach tends to choose timings with large timing error (larger than a symbol duration) because these erroneous timings have more accurate symbol timings. By contrast, the correlation based algorithm tends to choose timings close to the true timing but with symbol errors. Small errors in symbol timing only result in small SNR degradation, but large timing errors can probably lead to undetectable frame error. At very high SNR, since performance with lists of multiple entries coverages to that with list length of one, the performance of the ML-CPM approach will be better than that of the correlation approach.

The performance of a conventional decoder-assisted list synchronizer [20] is also shown in Fig. 7, where the receiver chooses the timing in the list that maximizes the LLF. Compared with the conventional scheme, the probability of frame error of the proposed receiver is lower by over one order of magnitude, at the affordable cost of slightly lower probability of successfully detection under higher SNR conditions. Further, the proposed receiver only requires a syndrome decoder, whereas the conventional approach requires a ML decoder, such as [28] used in the simulations, and LLF calculation [20].

V. CONCLUSION

An architecture and algorithms for the first all-digital receiver for radio-controlled clocks (RCCs) based on the enhanced WWVB broadcast format were proposed and analyzed. Two joint symbol and frame synchronization approaches, based on ML and correlation, were proposed to overcome the potential low SNR conditions and frequency offsets as large as 4 times the symbol rate. In particular, decision and detection strategies for tracking and acquisition operations were proposed and

analyzed. In tracking, simulation results show that by applying the proposed soft and hard decision strategies, the variance of timing error could be reduced by as much as 63%, providing a performance gain of 15 dB compared with a theoretical receiver based on envelope detection for the legacy broadcast, and an even larger gap when compared to typical available receivers without sophisticated digital processing. In acquisition, the performance of the synchronization operation could be improved by employing a joint decoding and synchronization scheme based on a list synchronizer. Simulation results show that the probability of successful detection is as high as 98% with probability of frame error being limited to about 10^{-4} at 8 dB SNR, indicating over 16 dB performance advantage over a theoretical envelope detection based receiver for the legacy broadcast. The trade-off between energy consumption and performance was studied and was shown to be controlled by varying the timing search interval in tracking and selecting a different list length for the list synchronization in acquisition. Future work should consider reception of other transmission modes with longer symbol durations and lower code rates, accommodating larger frequency drift and more challenging implementation complexity constraints.

APPENDIX A
SNR LOSS CAUSED BY APPROXIMATION OF LIKELIHOOD FUNCTION (5)

We assume coherent detection when calculating the SNR degradation. Let $g^{(0)}(t)$ and $g^{(1)}(t)$ denote the transmitted pulse shape for AM "0" and "1" respectively. In tracking, AM bits are deterministic, and therefore the optimal decision criteria for the kth bit in BPSK is given by:

$$\int_{kT}^{(k+1)T} r(t)g^{(0)}(t) \overset{'1'}{\underset{'0'}{\gtrless}} 0$$
$$\text{if } r(t) = g^{(0)}(t-kT) + w(t) \text{ for } kT \leq t < (k+1)T$$
$$\int_{kT}^{(k+1)T} r(t)g^{(1)}(t) \overset{'1'}{\underset{'0'}{\gtrless}} 0$$
$$\text{if } r(t) = g^{(1)}(t-kT) + w(t) \text{ for } kT \leq t < (k+1)T$$
$$(21)$$

where $r(t)$ is the timing synchronized received signal corrupted by zero-mean AWGN with variance $\sigma^2 = \frac{N_0}{2}$, and T is symbol duration. The resulting bit error rate (BER), P_b^{track}, is given by:

$$P_b^{track} = p^{(0)}Q\left(\sqrt{\frac{2E^{(0)}}{N_0}}\right) + p^{(1)}Q\left(\sqrt{\frac{2E^{(1)}}{N_0}}\right) \quad (22)$$

where $p^{(0)}$ and $p^{(1)}$ are the probabilities of the AM bit being "0" and "1", respectively. The energy per symbol for pulse shape $g^{(0)}(t)$ and $g^{(1)}(t)$ are $E^{(0)}$ and $E^{(1)}$, respectively.

In acquisition, AM bits are unknown at the receiver, but the distribution of different pulse shapes is known. Therefore, the

optimal receiver and decision criteria for BPSK is:

$$p^{(0)}e^{-\frac{E^{(0)}-2\int_0^T g^{(0)}(t)r(t)dt}{2\sigma^2}} + p^{(1)}e^{-\frac{E^{(1)}-2\int_0^T g^{(1)}(t)r(t)dt}{2\sigma^2}}$$

$$\underset{\text{`0'}}{\overset{\text{`1'}}{\gtrless}} p^{(0)}e^{-\frac{E^{(0)}+2\int_0^T g^{(0)}(t)r(t)dt}{2\sigma^2}} + p^{(1)}e^{-\frac{E^{(1)}+2\int_0^T g^{(1)}(t)r(t)dt}{2\sigma^2}}$$

$$p^{(0)}e^{-\frac{E^{(0)}}{2\sigma^2}}\sinh\left(\frac{\int 0^T g^{(0)}(t)r(t)dt}{\sigma^2}\right)$$

$$+ p^{(1)}e^{-\frac{E^{(1)}}{2\sigma^2}}\sinh\left(\frac{\int_0^T g^{(1)}(t)r(t)dt}{\sigma^2}\right) \underset{\text{`0'}}{\overset{\text{`1'}}{\gtrless}} 0 \quad (23)$$

Let Z denote the LHS of (23). Since the probability of "0" and "1" being transmitted in PM is equal, we assume "1" is transmitted in PM in the calculation of BER of criteria (23). Let A and P denote the transmitted AM bits and PM bits respectively. It can be shown that the conditional PDF of Z given $P = 1$ and $A = \{0,1\}$ is:

$$f_{Z|P=1,A=j}(z)$$

$$= \frac{1}{2\pi\sigma_1\sigma_2}\frac{1}{\alpha\beta}\int_{-\infty}^{\infty}\frac{1}{\sqrt{\left(\frac{w}{\alpha}\right)^2+1}\sqrt{\left(\frac{z-w}{\beta}\right)^2+1}}$$

$$\times e^{-\frac{\left(\sinh^{-1}(\frac{w}{\alpha})-\mu_1^{(j)}\right)^2}{2\sigma_1^2}-\frac{\left(\sinh^{-1}(\frac{z-w}{\beta})-\gamma\sinh^{-1}(\frac{w}{\alpha})-\mu_2^{(j)}\right)^2}{2\sigma_2^2}} \, dw$$

$$\quad (24)$$

where $\alpha = p^{(0)}e^{-\frac{E^{(0)}}{2\sigma^2}}$, $\beta = p^{(1)}e^{-\frac{E^{(1)}}{2\sigma^2}}$, $C = \frac{c_{01}}{c_{00}} = 0.68$, $\mu_1^{(0)} = \frac{E^{(0)}}{\sigma^2}$, $\mu_1^{(1)} = \frac{c_{00}c_{01}}{\sigma^2}$, $\sigma_1^2 = \frac{E^{(0)}}{\sigma^2}$, $\mu_2^{(0)} = 0$, $\mu_2^{(1)} = \frac{c_{11}^2}{\sigma^2}$, and $\sigma_2^2 = \frac{c_{11}^2}{\sigma^2}$. Note that $c_{ij} = \int_{-\infty}^{\infty}g^{(j)}(t)h^{(i)}(t)dt$ is the projection of waveform $g^{(j)}$ on basis $h^{(i)}$, where orthonormal basis set $h^{(0)}$ and $h^{(1)}$ is derived by the Gram-Schmidt process with $h^{(0)} = g^{(0)}/\sqrt{E^{(0)}}$. Therefore, the BER, P_b^{acq}, for the optimal decision criteria for acquisition given by (23) is:

$$P_b^{acq} = p^{(0)}\int_{-\infty}^{0}f_{Z|P=1,A=0}(z)\,dz + p^{(1)}\int_{-\infty}^{0}f_{Z|P=1,A=1}(z)\,dz$$

$$\quad (25)$$

To reduce the implementation complexity of the receiver in both tracking and acquisition operations, we propose a simplified decision criterion, given by:

$$\int_0^T r(t)\bar{g}(t) \underset{\text{"0"}}{\overset{\text{"1"}}{\gtrless}} 0 \quad (26)$$

where $\bar{g}(t) = \frac{1}{2}(g^{(0)}(t) + g^{(1)}(t))$. The resulting BER, P_b^{sim} is given by:

$$P_b^{sim} = p^{(0)}Q\left(\sqrt{\frac{2E^{(0)'}}{N_0}}\right) + p^{(1)}Q\left(\sqrt{\frac{2E^{(1)'}}{N_0}}\right) \quad (27)$$
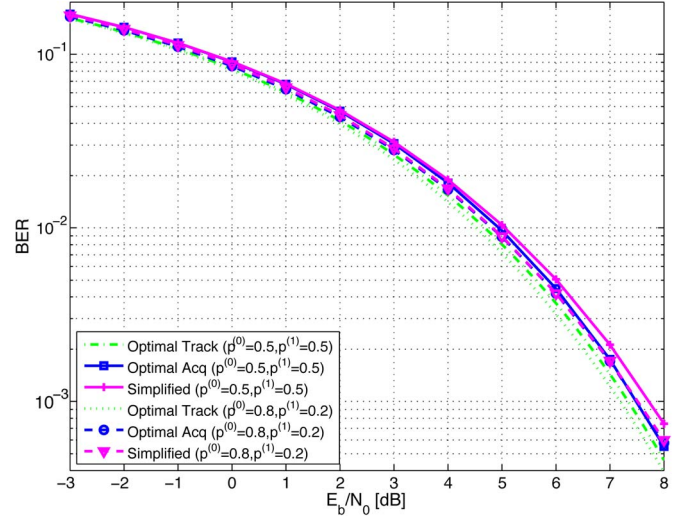

Fig. 8. BER comparison of the optimal decision criteria (21), (23) and simplified decision criterion (26).

where $E^{(j)'}$ is the energy per bit at the output of the demodulation filter, and $E^{(j)'} = \frac{(\int_0^T g^{(j)}(t)\bar{g}(t)dt)^2}{\int_0^T \bar{g}^2(t)dt}$ for $j \in \{0,1\}$.

To quantify the average performance degradation in tracking and in acquisition, Fig. 8 shows the optimal BER in tracking (22), optimal BER in acquisition (25) and BER of the simplified criteria for both operations (27), assuming two distributions of AM "0" and "1": smallest $p^{(0)}$ and largest $p^{(0)}$ within all AM bits. The x-axis of Fig. 8 represents the average SNR per bit E_b/N_0, where $E_b = p^{(0)}E^{(0)} + p^{(1)}E^{(1)}$. Fig. 8 indicates that the simplified approach introduces marginal SNR degradation compared with the optimal approaches in both distributions. The comparison shown in Fig. 8 implicitly assumes that all the AM bits are unknown and that the random PM data carries the same amount of information about frequency and timing as that of the sync word. In reality, however, there are known AM bits (marker and reserved bits "0") and the Fisher information of the sync word is larger than that of random data, as shown by Appendix C. Therefore, the actual SNR degradation introduced by the simplified approach is even lower than that shown in Fig. 8.

APPENDIX B
EFFECT OF LIST LENGTH ON PROBABILITY OF FRAME ERROR AND SUCCESSFUL DETECTION

The event of frame error or successful detection occurs if the Hamming (31,26) decoder produces a zero syndrome based on any of the timings in the list. Therefore, given any received signal r and the syndrome S_α based on the α-th timing in the length-ν list, the probability of frame error or successful detection is given by:

$$P_{Y|r}(\nu) = \Pr(Y, S_1 = 0|r) + \Pr(Y, S_1 \neq 0, S_2 = 0|r) + \ldots$$

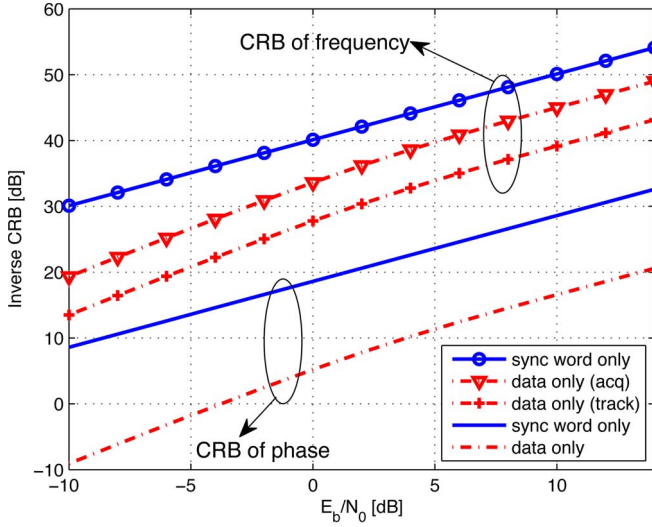$$+ \Pr(Y, S_1 \neq 0, \ldots, S_{\nu-1} \neq 0, S_\nu = 0|r) \quad (28)$$

Fig. 9. Inverse CRB of frequency and phase based on received sync word and received data, where inverse CRB in dB scale is calculated by $10\log_{10} \frac{1}{CRB}$.

where $Y = \{det, fe\}$ for event of successful detection and frame error. If the list length increases by 1, it is clear that

$$P_{Y|r}(\nu + 1) = P_{Y|r}(\nu) + \Pr(Y, S_1 \neq 0, \dots, S_\nu \neq 0, S_{\nu+1} = 0|r) > P_{Y|r}(\nu) \tag{29}$$

Since $P_{era} = 1 - P_{fe} - P_{det}$, the overall probability of successful detection and frame error increase as ν increases, and the overall probability of erasure decreases as ν increases.

APPENDIX C
CRAMÉR-RAO BOUND OF THE FREQUENCY AND PHASE BASED ON THE RECEIVED SYNC WORD AND DATA

Given the correct timing m, the joint Fisher information, F, of frequency and phase is given by [29]:

$$F = \frac{2E_s}{N_0} \begin{bmatrix} 4\pi^2 T_s^2 \check{\delta} & 2\pi T_s \check{\iota} \\ 2\pi T_s \check{\iota} & \varepsilon \end{bmatrix} \tag{30}$$

For estimation based on the received sync word, $\check{\delta} = \sum_{k=0}^{Nl_{sw}-1} k^2 |c_k|^2$, $\check{\iota} = \sum_{k=0}^{Nl_{sw}-1} k |c_k|^2$, and $\varepsilon = \sum_{k=0}^{Nl_{sw}-1} |c_k|^2$. For estimation based on l_d received data symbols, $\check{\delta} = \sum_{i\in\mathcal{D}} \sum_{l\in\gamma_i} l^2 |d_l^{(i)}|^2 (1 - 2P_b(\rho))$, $\check{\iota} = \sum_{i\in\mathcal{D}} \sum_{l\in\gamma_i} l |d_l^{(i)}|^2 (1 - 2P_b(\rho))$, and $\varepsilon = \sum_{i\in\mathcal{D}} \sum_{l\in\gamma_i} |d_l^{(i)}|^2 (1 - 2P_b(\rho))$, where set $\mathcal{D} \cap \Psi_m = \emptyset$ and its cardinality $|\mathcal{D}| = l_d$. The probability of bit error under SNR $\rho = \frac{E_b}{N_0}$, $P_b(\rho)$, is given by (27).

The CRB of frequency is $\text{var}(\Delta f) \geq F_{11}^{-1}$, where $l_d = l_f - l_{sw}$ for acquisition and $l_d = 2t_s$ for tracking. Since a direct-form phase estimation can only be derived from one term in (6), the CRB of phase is $\text{var}(\phi_0) \geq F_{22}^{-1}$, and $l_d = 1$. In Fig. 9, the data bits used in estimation are assumed to be all "0" in AM to simplify the calculation, i.e., $d_l^{(i)} = d_l^{[0]} \forall i \in \mathcal{D}$. Despite this assumption in favor of estimation based on received data, the CRB of both frequency and phase are better for estimation based on the received sync word than for that based on the received data.

REFERENCES

[1] J. Lowe *et al.*, "New improved system for WWVB broadcast," in *Proc. 43rd Annu. PTTI Meet.*, 2011, pp. 163–184.

[2] Y. Liang, D. Rajan, O. Eliezer, S. Balasubramanian, and W. Khalil, "A new broadcast format and receiver architecture for radio controlled clocks," in *Proc. IEEE MWSCAS*, Columbus, OH, USA, 2013, pp. 1128–1131.

[3] Y. Liang, O. Eliezer, D. Rajan, and J. Lowe, "WWVB time signal broadcast: An enhanced broadcast format and multi-mode receiver," *IEEE Commun. Mag.*, vol. 52, no. 5, pp. 210–217, May 2014.

[4] M. Chiani, "Noncoherent frame synchronization," *IEEE Trans. Commun.*, vol. 58, no. 5, pp. 1536–1545, May 2010.

[5] Z. Y. Choi and Y. Lee, "Frame synchronization in the presence of frequency offset," *IEEE Trans. Commun.*, vol. 50, no. 7, pp. 1062–1065, Jul. 2002.

[6] B. Ramakrishnan, "Frame synchronization with large carrier frequency offsets: Point estimation versus hypothesis testing," in *Proc. IEEE CSNDSP*, 2010, pp. 45–50.

[7] Y. Koo and Y. Lee, "A joint maximum likelihood approach to frame synchronization in presence of frequency offset," in *Proc. IEEE ICC*, 2002, pp. 1546–1550.

[8] J. Gansman, M. Ftiz, and J. Krogmeier, "Optimum and suboptimum frame synchronization for pilot-symbol-assisted modulation," *IEEE Trans. Commun.*, vol. 45, no. 10, pp. 1327–1337, Oct. 1997.

[9] R. Pedone and M. Villanti, "Frame synchronization in frequency uncertainty," *IEEE Trans. Commun.*, vol. 58, no. 4, pp. 1235–1246, Apr. 2010.

[10] M. Villanti, P. Salmi, and G. E. Corazza, "Differential post detection integration techniques for robust code acquisition," *IEEE Trans. Commun.*, vol. 55, no. 11, pp. 2172–2184, Nov. 2007.

[11] G. Corazza and R. Pedone, "Generalized and average likelihood ratio testing for post detection integration," *IEEE Trans. Commun.*, vol. 55, no. 11, pp. 2159–2171, Nov. 2007.

[12] J. Lowe, Enhanced WWVB Broadcast Format, Nat. Inst. Standards Technol., Boulder, CO, USA. [Online]. Available: http://www.nist.gov/pml/div688/grp40/wwvb.cfm

[13] J. Massey, "Optimum frame synchronization," *IEEE Trans. Commun.*, vol. COM-20, no. 2, pp. 115–119, Apr. 1972.

[14] D. Rife and R. Boorstyn, "Single tone parameter estimation from discrete-time observations," *IEEE Trans. Inf. Theory*, vol. 20, no. 5, pp. 591–598, Sep. 1974.

[15] S. Umesh and D. Nelson, "Computationally efficient estimation of sinusoidal frequency at low SNR," in *Proc. IEEE ICASSP*, 1996, pp. 2797–2800.

[16] T. Brown and M. Mao Wang, "An iterative algorithm for single-frequency estimation," *IEEE Trans. Signal Process.*, vol. 50, no. 11, pp. 2671–2682, Nov. 2002.

[17] U. Mengali and M. Morelli, "Data-aided frequency estimation for burst digital transmission," *IEEE Trans. Commun.*, vol. 45, no. 1, pp. 23–25, Jan. 1997.

[18] R. Kinsman, "Temperature compensation of crystals with parabolic temperature coefficients," in *Proc. IEEE Annu. Symp. Frequency Control*, 1978, pp. 102–107.

[19] D. Pauluzzi and N. Beaulieu, "A comparison of SNR estimation techniques for the AWGN channel," *IEEE Trans. Commun.*, vol. 48, no. 10, pp. 1681–1691, Oct. 2000.

[20] P. Robertson, "A generalized frame synchronizer," in *Proc. IEEE GLOBECOM*, 1992, pp. 365–369.

[21] P. Robertson, "Improving frame synchronization when using convolutional codes," in *Proc. IEEE GLOBECOM*, 1993, pp. 1606–1611.

[22] M. Howlader and B. Woerner, "Decoder-assisted frame synchronization for packet transmission," *IEEE J. Sel. Areas Commun.*, vol. 19, no. 12, pp. 2331–2345, Dec. 2001.

[23] T. Cassaro and C. Georghiades, "Frame synchronization for coded systems over AWGN channels," *IEEE Trans. Commun.*, vol. 52, no. 3, pp. 484–489, Jan. 2004.

[24] X. Luo and M. Howlader, "Noncoherent decoder-assisted frame synchronization for packet transmission," *IEEE Trans. Wireless Commun.*, vol. 5, no. 5, pp. 961–966, May 2006.

[25] M. Howlader, "Decoder-assisted channel estimation and frame synchronization of turbo coded systems," in *Proc. IEEE VTC Spring*, 2002, vol. 3, pp. 1452–1456.

[26] Z. Chen and J. Yuan, "A code-aided soft frame synchronization algorithm for quasi-cyclic LDPC coded system," in *Proc. IEEE IWCMC*, Sep. 2009, pp. 1–4.

[27] H. Wymeersch and H. Steendam, "Code-aided frame synchronization and phase ambiguity resolution," *IEEE Trans. Signal Process.*, vol. 54, no. 7, pp. 2747–2757, Jul. 2006.

[28] T. Kaneko, T. Nishijima, H. Inazumi, and S. Hirasawa, "An efficient maximum-likelihood-decoding algorithm for linear block codes with algebraic decoder," *IEEE Trans. Inf. Theory*, vol. 40, no. 2, pp. 320–327, Mar. 1994.

[29] T. Schonhoff and A. Giordano, *Detection and Estimation Theory*. Englewood Cliffs, NJ, USA: Prentice-Hall, 2006.

Dinesh Rajan (S'99–M'02–SM'07) received the B.Tech. degree in electrical engineering from the Indian Institute of Technology (IIT), Madras, India, and the M.S. and Ph.D. degrees in electrical and computer engineering from Rice University, Houston, TX, USA. He is currently the Department Chair and Cecil and Ida Green Professor of the Department of Electrical Engineering, Southern Methodist University (SMU), Dallas, TX. His current research interests include communications theory, wireless networks, information theory, and computational imaging. He was a recipient of the National Science Foundation CAREER Award for his work on applying information theory to the design of mobile wireless networks.

Yingsi Liang (S'14) received the B.E. degree in communication engineering from the South China Normal University, Guangzhou, China, in 2008 and the M.S. and Ph.D. degrees in electrical engineering from the Southern Methodist University, Dallas, TX, USA, in 2010 and 2014, respectively. Her research has resulted in major contributions to the design of the enhanced WWVB broadcast, which the National Institute of Standards and Technology (NIST) has deployed in 2012, as well as to the development of the EverSet receiver technology for this broadcast.

Her research interests include wireline and wireless communication systems, synchronization, channel coding, interference mitigation, and digital signal processing.

Oren Eliezer (M'98–SM'14) received the B.S.E.E. and M.S.E.E. degrees majoring in communication theory, digital signal processing, and control systems from Tel Aviv University, Tel Aviv, Israel, in 1988 and 1996, respectively, and the Ph.D. degree in microelectronics from The University of Texas at Dallas, Richardson, TX, USA, in 2008.

From 1988 to 1994, he served in the Israel Defense Forces, where he specialized in wireless communications, and after his military service, he cofounded Butterfly VLSI, Ltd., where he served as the Chief Engineer. Following its acquisition by Texas Instruments (TI) in 1999, he was relocated to Dallas in 2002, where he took part in the development of TI's Digital RF Processor (DRP^{TM}) technology and was elected as a Senior Member of the Technical Staff. Since 2009, he has been serving as the Chief Technology Officer for Xtendwave (now EverSet Technologies), Dallas, where he has led the development of the enhanced WWVB broadcast and the EverSet receiver technology for it. He has authored and coauthored over 50 journal and conference papers and over 30 issued patents and has given over 50 invited talks and seminars related with communication systems, digital transceiver architectures, interference mitigation, built-in testing, and built-in calibration and compensation in wireless transceiver integrated circuits.

Dr. Eliezer serves on advisory boards for academia and on steering committees of several IEEE conferences, and he was a recipient of the IEEE Circuits and Systems Award for outstanding voluntary work in his region in 2010.